Supporting Information

Phatnani et al. 10.1073/pnas.1222361110

SI Materials and Methods

Glia Dissection. Glia monolayers were obtained essentially as described previously (1). Tissue was isolated in calcium- and magnesium-free HBSS. Under a dissecting microscope, the cortex was isolated and carefully stripped of the meninges. The tissue was minced into small pieces and transferred to a 50-mL centrifuge tube in a final volume of 12 mL HBSS. Tissue digestion was performed using trypsin-EDTA (GIBCO) and 1% DNase (Sigma) at 37 °C for 15 min, swirling the mixture periodically. Dissociated tissue was triturated using a fire-polished Pasteur glass pipette and filtered through a 72-m nylon mesh (NITEX 100% polyamide nylon fiber; TETKO) to remove any undissociated tissue. Filtered material was pelleted at 300 × *g* for 5 min and resuspended in 2 mL glia medium [Minimum Essential Medium with Earl's salts (GIBCO), 20% glucose, penicillin-streptomycin (GIBCO), 10% horse serum (GIBCO)], and the cell number was determined. One brain generally yielded enough glia to plate one T25 flask (Falcon). After monolayers were confluent (generally in 7 d), cells were replated on 24-well multiwell dishes that had been coated with poly-D-lysine (0.5 mg mL^{-1} for 30 min at 21–25 °C).

Differentiation of ES Cells into Motor Neurons and Sandwich Culture. Mouse ES cells were differentiated into motor neurons according to methods previously described (1, 2). The ES cells were grown over mouse embryonic fibroblasts (Millipore) to 70–80% confluence in 15-cm plates (Corning) in mouse ES cell medium [DMEM; EmbryoMax (Specialty Media), 10% knockout serum replacement, penicillin, streptomycin, glutamine (GIBCO), 2-mercaptoethanol, nonessential amino acids, leukemia inhibitory factor (Chemicon)]. To form embryoid bodies, cells were washed one time with PBS and then incubated with 3 mL prewarmed 0.25% trypsin (GIBCO) for 5 min at 37 °C. Cells were then resuspended in 10 mL DFNK medium [3 parts DMEM:1 part F12 (GIBCO), 10% knockout serum replacement (GIBCO), penicillin, streptomycin, glutamine (GIBCO), 2-mercaptoethanol (GIBCO)], counted, and plated at a concentration of ∼200,000 cells/mL in 15-cm dishes (Corning). Two days later, embryoid bodies were split from one dish into two Petri dishes (Fisher) containing DFNK medium supplemented with retinoic acid (100 nM; stock: 1 mM in DMSO; Sigma) and Sonic hedgehog (500 nM agonist Ag 1.3 from Curis; gift of Lee Rubin, Harvard University, Cambridge, MA).

On day 5, the embryoid bodies were dissociated into single-cell suspensions. The embryoid bodies were pelleted in a 15-mL Falcon tube, washed one time with PBS, and incubated in Earle's balanced salt solution with 20 units papain and 1,000 units DNase I (Worthington Biochemical) for 30 min at 37 °C. The mixture was then triturated with a 5-mL pipette and centrifuged for 5 min at 400 × *g*. The resulting cell pellet was washed with PBS, resuspended in F12 medium [F12 medium (GIBCO) with 2% horse serum and penicillin-streptomycin (GIBCO)], and FACS-purified using a MoFlo XDP cell sorter from Beckman Coulter. The cell suspension was centrifuged for 5 min at 400 × *g*, and the resulting cell pellet was washed with PBS and resuspended in motor neuron medium [F12 medium (GIBCO) with 5% horse serum and penicillin-streptomycin (GIBCO), B-27 supplement (GIBCO), N2 supplement (GIBCO)] with neurotrophic factors [glial cell line-derived neurotrophic factor (GDNF), ciliary neurotrophic factor (CNTF), neurotrophin-3 (NT3), and brain-derived neurotrophic factor (BDNF); 10 ng/mL; R&D Systems]. The cells were counted and plated on poly-D-lysine/laminin 12-mm coverslips (BD Biosciences) with paraffin wax feet (described in ref. 3). The coverslips were incubated for 60 min at 37 °C and inverted over a layer of primary glia cells in 24-well dishes. Culture medium was changed after ∼12 h and then, every 2 d. Cells were harvested at different time points after plating (7, 14, and 21 d). To harvest RNA, coverslips with neurons were transferred to wells containing TRIzol, and the TRIzol solution was triturated with a pipette and transferred to a microcentrifuge tube. For glial RNA, medium was aspirated after the neuron-containing coverslips had been transferred to TRIzol, and TRIzol was added to the wells containing the glia. The solution was triturated with a pipette and transferred to a microcentrifuge tube. RNA was extracted immediately, or the tubes were stored at −80 °C.

Spinal Cord Dissection for RNA. Anesthetized mice were decapitated, the spinal column was severed just above the sacrum, and spinal cords were extruded into a beaker using a 10-mL syringe attached to an 18-gauge 1 1/2 beveled needle. Each spinal cord was transferred to a microcentrifuge tube containing 1 mL TRIzol, minced into pieces, and then triturated further using a series of needles of increasing gauge (18–23 gauge) attached to a 1-mL syringe. RNA was extracted immediately, or the tubes were stored at −80 °C.

RNA Extraction and cDNA Library Preparation. Two hundred fifty microliters chloroform per one milliliter TRIzol were added to each tube. Tubes were then vortexed at maximum speed for 15 s, incubated at room temperature for 2–3 min, and centrifuged at 12,000 × *g* for 15 min at 4 °C. The aqueous phase was transferred to new tubes, to which an equal volume of 70% ethanol was slowly added with frequent mixing. This mixture was then applied to an RNeasy column (Qiagen), which was then washed and from which RNA was eluted according to the manufacturer's instructions. RNA was eluted in a final volume of 32 μL. Libraries were prepared using either standard protocols from Illumina or the Nextera transposase-mediated method (4) and sequenced using the Illumina platform.

RNA Sequencing Data Analysis. Sequenced reads were mapped to the mouse genome sequence [University of California at Santa Cruz (UCSC) mm9] and also a library of known exon–exon junctions using bowtie. Both aligned and junction reads were then annotated against the UCSC known gene set (5). Reads per kilobase per million mapped reads (RPKM) values of raw read counts were calculated using DESeq (6). All these individual steps were carried out in an automated fashion using ExpressionPlot (7), which was also used to generate the two- (comparing RPKM values) and four-way (comparing RPKM ratios) plots and empirical cumulative distribution functions.

Quantitative PCR Analysis of Glia RNA. Aliquots of the same RNA used for RNA sequencing (RNA-Seq) analysis for one WT and one mutant (MT) glia sample were used to confirm the technical fold changes. Quantitative PCR (qPCR) analysis was carried out as described (8) using equal RNA input amounts. For qPCR, $\log_2$(fold changes) was calculated as C_t[WT] − C_t[MT], and error bars indicate SD of technical triplicates. For RNA-Seq plot, $\log_2$(fold changes) is calculated as log ratios of RPKMs. Error bars indicate SE of this ratio from Monte Carlo simulation of the ratio of two Poisson processes. All primer sequences are shown in Table S1.

Hierarchical Clustering of Sandwich Culture Samples. To ensure consistency when comparing data from different platforms, we summarized expression values to the gene level (i.e., for genes having more than one isoform, we calculated the sum of RPKMs across samples for each transcript, and then, we selected as the

most representative the one with the highest value). We then performed hierarchical clustering using Pearson correlation as similarity metric and single linkage (i.e., shortest distance) as the linkage method. The analysis was performed within the R\Bioconductor statistical framework (9, 10).

Heat Map with Cell Type-Specific Gene Subsets. We performed hierarchical clustering using Spearman rank correlation on sandwich samples using cell type-specific signature genes modified from Cahoy et al. (11) and Lei et al. (12). RPKM expression levels were $\log_2 z$ score-transformed.

Heat Map with Cell Type-Specific Gene Expression Profiles. Gene expression profiles from different platforms were normalized as follows: Affymetrix 430v2 and MoEx were background-corrected, summarized, and normalized using multiarray average (13) from *affy* (14) and *oligo* (15) functions, respectively. We then collapsed the data to gene-level expression by selecting probes with the highest interquartile range. We estimated the overall similarity between sandwich samples and those samples from different datasets by computing the Spearman rank correlation. We then hierarchically clustered the coefficients and visualized the clusters as a heat map.

Functional Analyses. To perform functional enrichment analysis, we used (*i*) Ingenuity Pathway Analysis (Ingenuity Systems; www.ingenuity.com), which assesses statistical significance using right-tailed Fisher exact test to calculate a *P* value determining the probability that each biological function and/or disease assigned to that dataset is caused by chance alone, and (*ii*) Pathway Guide (Advaita Corporation; www.advaitacorporation.com) (16, 17). For each individual analysis, we used a list of significant genes exploiting fold change and *P* value as calculated by ExpressionPlot. To compare the effects on KEGG pathways in the different conditions, we combined the results from Pathway Guide and compared the total accumulations as a measure of perturbation within each set.

Immunofluorescence Studies: Immunocytochemistry Analyses. Immunocytochemistry analyses were performed essentially as described previously (1). Cells were fixed with 4% paraformaldehyde-PBS, blocked, and permeabilized with BSA (1%)-Triton X-100 (0.1%). They were then incubated overnight with the following antibodies: mouse monoclonal antineuronal β-III tubulin (Covance), rabbit anti-GFP (Alexa488-conjugated; Molecular Probes), or rabbit anti-GFAP (Chemicon). The cells were then incubated with donkey antibodies specific for rabbit, conjugated to Cy3 (1:100, 2 h; Jackson ImmunoResearch) and/or donkey antibodies specific for mouse, and conjugated to Cy5 antibodies (1:100, 2 h; Jackson ImmunoResearch). After the samples were mounted in Vectashield (Vector Labs), confocal or epifluorescence microscopy was performed using Olympus FV 1000 (40× and 60× oil immersion objective, 1.45 N.A.) or Olympus IX70. Image acquisition was performed using FLUOVIEW software 4.0 (Olympus). For relative fluorescence analysis, all settings, such as exposure time, magnification, and gain, were maintained constant for all samples. Offline analysis of relative intensities for all of the samples was done using Metamorph 4.5 (Universal Imaging). Only cells having morphological features of neurons (that is, phase bright soma and several neurites) were considered for subsequent analysis.

Immunofluorescence Studies: Immunohistochemistry Analyses. ***Tissue preparation.*** After i.p. injection of anesthetic (avertin, 0.1 mg/mL; Sigma), mice at different ages (6, 8, 10, 12, and 16–17 wk) were heart-perfused with 20 mL 4%-p-formaldehyde in PBS (0.1 M, pH 7.4). Spinal cords were removed and further postfixed [overnight (ON)] in the same fixative at 4°C. The lumbar segments (L2–L5) were then incubated with sucrose (5%, 1 h; 15%, 4 h; 30%, ON) and soaked in optimal cutting temperature (OCT) tissue Tek compound (Leica). Blocks were frozen in dry ice and stored at −80°C until sectioning. The frozen lumbar segments were sectioned (50 μm) in a Leica CM1900 Cryostat (Leica) at −20°C, and the sections were collected on SuperFrost Plus slides (Fisher) and saved at −20°C for later immunolabeling.
Immunolabeling. Lumbar spinal cord cryoprotected sections were washed in 0.1 M PBS, pH 7.4, and incubated for 3–4 h with BSA (1%; Sigma) and Triton X-100 (0.1%; Sigma) in PBS to block unspecific binding. Sections were incubated ON with specific primary antibodies: anticholine acetyl transferase (CHAT; goat: 1/100; Invitrogen), antireceptor for TGFβ ligand type II (TGFβ-RII; rabbit: 1/250; Novus Biologicals), or anti-GFAP (rabbit: 1/500; DAKO or mouse: 1/200; Millipore). After several washes in PBS, sections were incubated for 4 h at room temperature with species-specific secondary antibodies (Alexa488–anti-goat: 1/1,000; Alexa594–anti-rabbit: 1/1,000; and Alexa594–anti-mouse: 1/500; Invitrogen). After several washes in 0.1 M PBS, immunostained sections were soaked in Vectashield (Vector Laboratories) and sealed with coverslips no. 1 (Fisher). An Olympus FluoView FV1000 confocal microscope equipped with a high N.A. (1.42) oil objective (60×) and Argon (488) and He-Ne (543) lasers was used to excite and collect the appropriated Alexa dyes (488 and 594).
Quantification of motor neurons. Counts of $SOD1^{G93A}$ motor neurons were performed at 6, 8, 10, 14, and 17 wk of age and compared with age-matched WT littermates. Cell counts were obtained by tracking (ImageJ; National Institutes of Health) ChAT-positive motor neurons from optical stacks covering the entire ventral horn. The ChAT motor neurons expressing TGFβ-RII were also annotated in these stacks. Prevalence was determined by dividing TGFβ-RII motor neurons by all ChAT neurons. A minimum of three sections per age was analyzed. Average cell counts were obtained from five $SOD1^{G93A}$ animals. One-way ANOVA with $P < 0.05$ was used for statistical comparisons. Results were expressed as mean ± SE.

1. Di Giorgio FP, Carrasco MA, Siao MC, Maniatis T, Eggan K (2007) Non-cell autonomous effect of glia on motor neurons in an embryonic stem cell-based ALS model. *Nat Neurosci* 10(5):608–614.
2. Wichterle H, Lieberam I, Porter JA, Jessell TM (2002) Directed differentiation of embryonic stem cells into motor neurons. *Cell* 110(3):385–397.
3. Kaech S, Banker G (2006) Culturing hippocampal neurons. *Nat Protoc* 1(5): 2406–2415.
4. Gertz J, et al. (2012) Transposase mediated construction of RNA-seq libraries. *Genome Res* 22(1):134–141.
5. Dreszer TR, et al. (2012) The UCSC Genome Browser database: Extensions and updates 2011. *Nucleic Acids Res* 40(Database issue):D918–D923.
6. Anders S, Huber W (2010) Differential expression analysis for sequence count data. *Genome Biol* 11(10):R106.
7. Friedman BA, Maniatis T (2011) ExpressionPlot: A web-based framework for analysis of RNA-Seq and microarray gene expression data. *Genome Biol* 12(7): R69.
8. Makeyev EV, Zhang J, Carrasco MA, Maniatis T (2007) The MicroRNA miR-124 promotes neuronal differentiation by triggering brain-specific alternative pre-mRNA splicing. *Mol Cell* 27(3):435–448.
9. Gentleman RC, et al. (2004) Bioconductor: Open software development for computational biology and bioinformatics. *Genome Biol* 5(10):R80.
10. R Development Core Team (2012) *R: A Language and Environment for Statistical Computing* (R Foundation for Statistical Computing, Vienna).
11. Cahoy JD, et al. (2008) A transcriptome database for astrocytes, neurons, and oligodendrocytes: A new resource for understanding brain development and function. *J Neurosci* 28(1):264–278.
12. Lei L, et al. (2011) Glioblastoma models reveal the connection between adult glial progenitors and the proneural phenotype. *PLoS One* 6(5):e20041.
13. Irizarry RA, et al. (2003) Exploration, normalization, and summaries of high density oligonucleotide array probe level data. *Biostatistics* 4(2):249–264.
14. Gautier L, Cope L, Bolstad BM, Irizarry RA (2004) affy—analysis of Affymetrix GeneChip data at the probe level. *Bioinformatics* 20(3):307–315.
15. Carvalho BS, Irizarry RA (2010) A framework for oligonucleotide microarray preprocessing. *Bioinformatics* 26(19):2363–2367.
16. Khatri P, Draghici S, Ostermeier GC, Krawetz SA (2002) Profiling gene expression using onto-express. *Genomics* 79(2):266–270.
17. Draghici S, Khatri P, Martins RP, Ostermeier GC, Krawetz SA (2003) Global functional profiling of gene expression. *Genomics* 81(2):98–104.

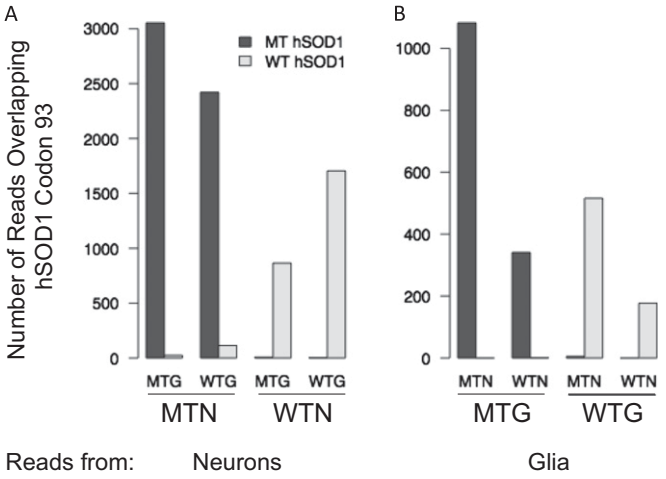

Fig. S1. Assessing the cell type specificity of sorted sandwich samples. Absolute numbers of RNA-Seq reads mapping to codon 93 of human superoxide dismutase (*SOD1*) were quantified in RNA samples obtained from (*A*) WT (WTNs) or G93A mutant neurons (MTNs) grown over WT (WTG) or mutant glia (MTG) and (*B*) WT (WTG) or mutant glia (MTG) grown under WT (WTNs) or G93A mutant neurons (MTNs). Reads mapping to WT or mutant codon 93 in all MT/WT combinations (WTN/MTG, MTN/WTG, MTG/WTN, and WTG/MTN) were used to assess the extent of cross-contamination between glia and neuron samples.

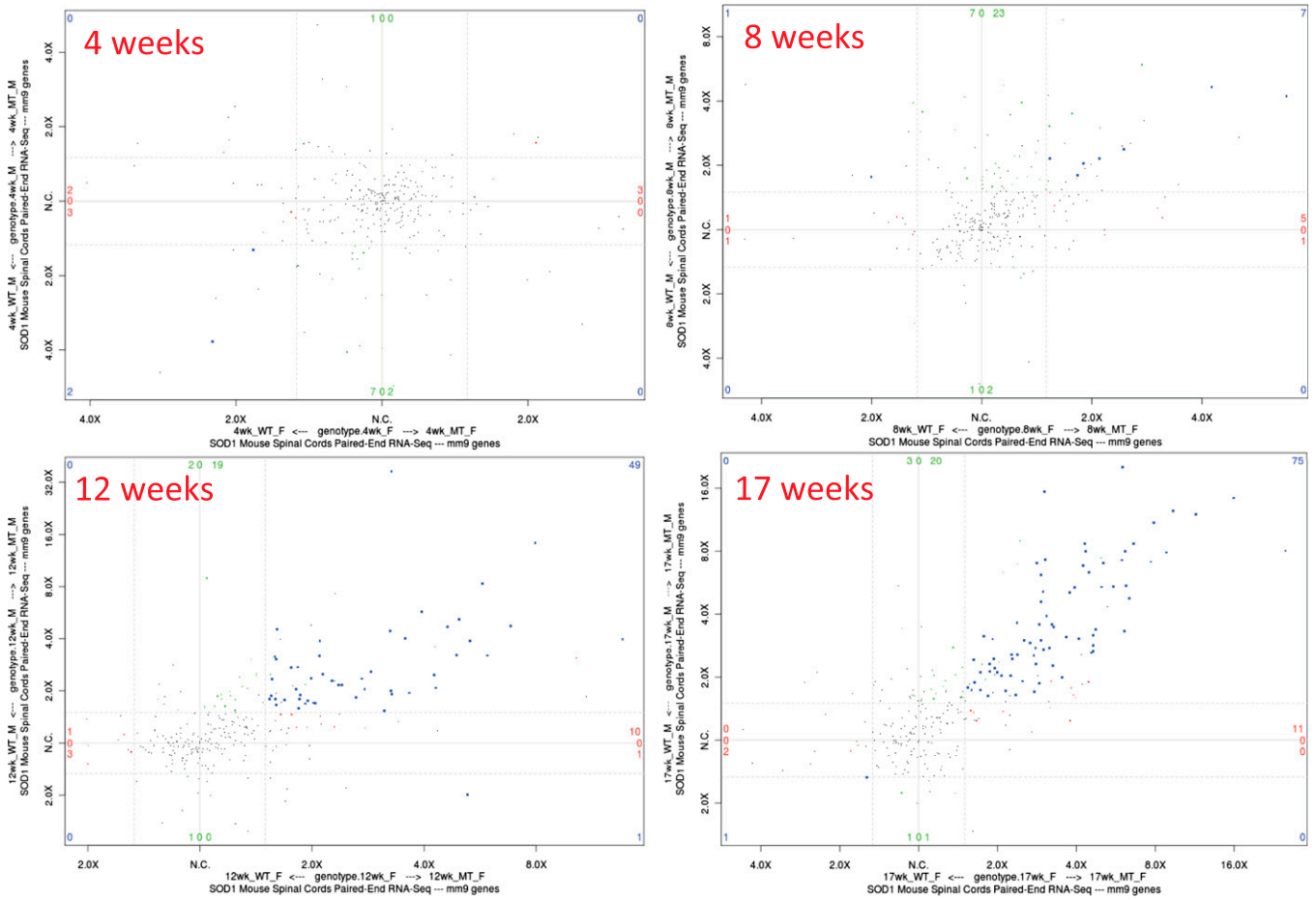

Fig. S2. Progressive up-regulation of cultured astrocyte genes in spinal cords; 159 cultured astrocyte-specific genes are overlaid onto four-way comparison plots of expression changes in male vs. female spinal cords at each of four time points along the disease course. Fold changes in expression (G93A relative to WT) in male spinal cords are plotted against changes in female spinal cords. Blue dots represent changed genes that meet the cutoff for statistical significance ($P < 0.001$, fold change > 1.5) in both male and female spinal cords. Blue dots in the upper right quadrant are genes expressed at higher levels in both male and female G93A spinal cords.

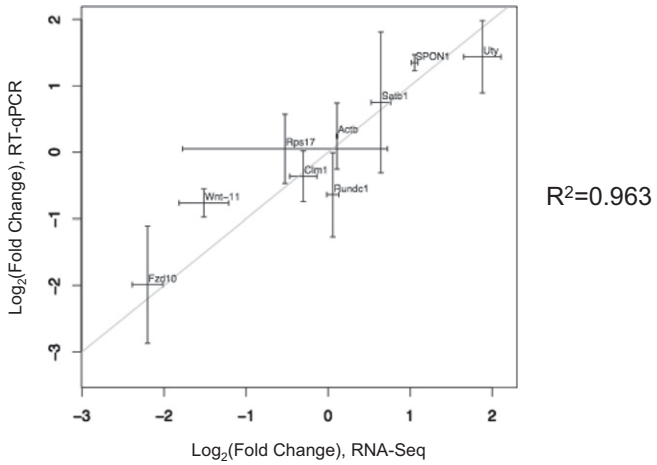

Fig. S3. Correlation plot of fold changes by RT-qPCR vs. fold changes by RNA-Seq. qPCR $\log_2$ (fold changes) was calculated as C_t[WT] − C_t[MT], and error bars indicate SD of technical triplicates, whereas for the RNA-Seq plot, $\log_2$ (fold changes) was calculated as log ratios of RPKMs. Error bars indicate SE of this ratio from Monte Carlo simulation of the ratio of two Poisson processes.

A: ECM Receptor Interaction

Glia

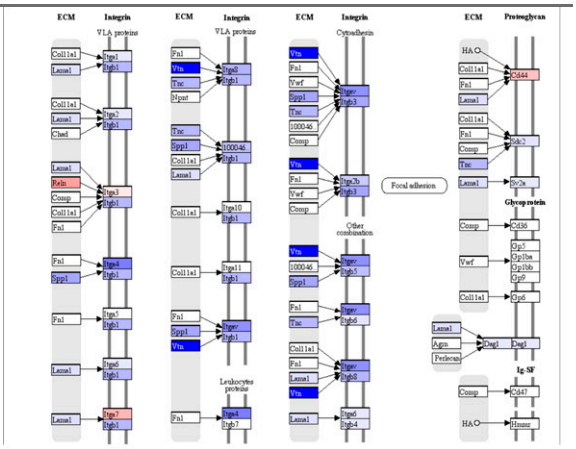

Cell Autonomous

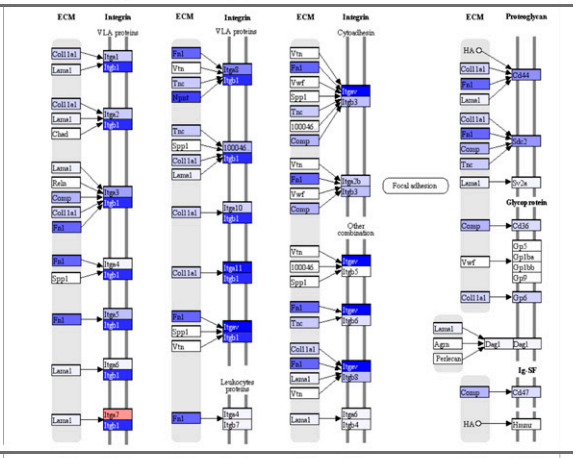

Non-Cell Autonomous

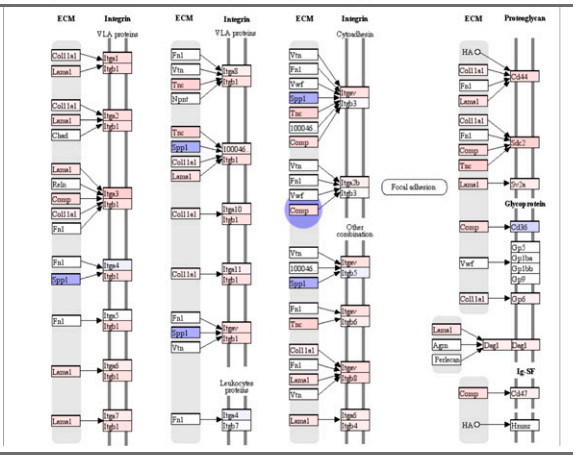

Fig. S4. (Continued)

B: Focal Adhesion	
Glia	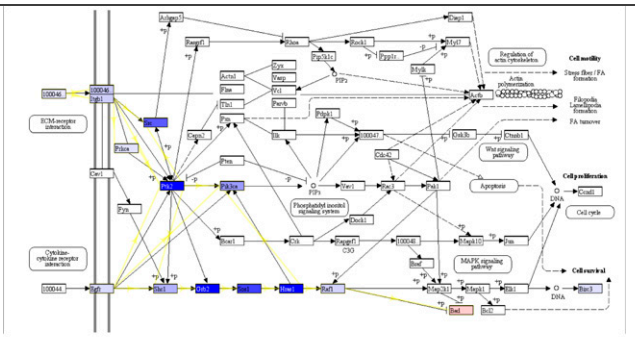
Cell Autonomous	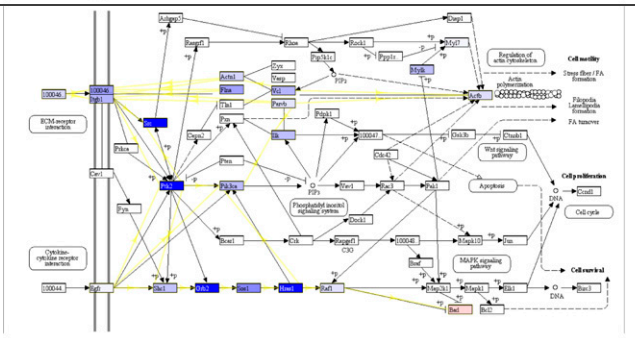
Non-Cell Autonomous	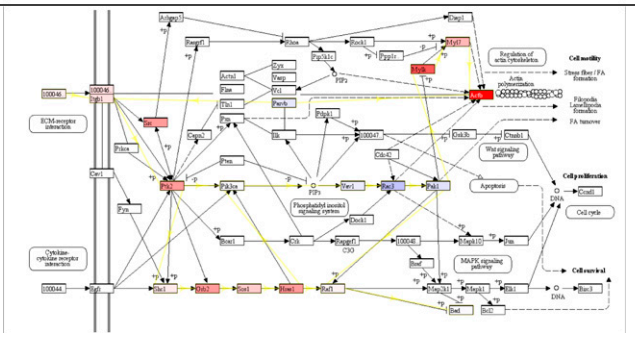

Fig. S4. (Continued)

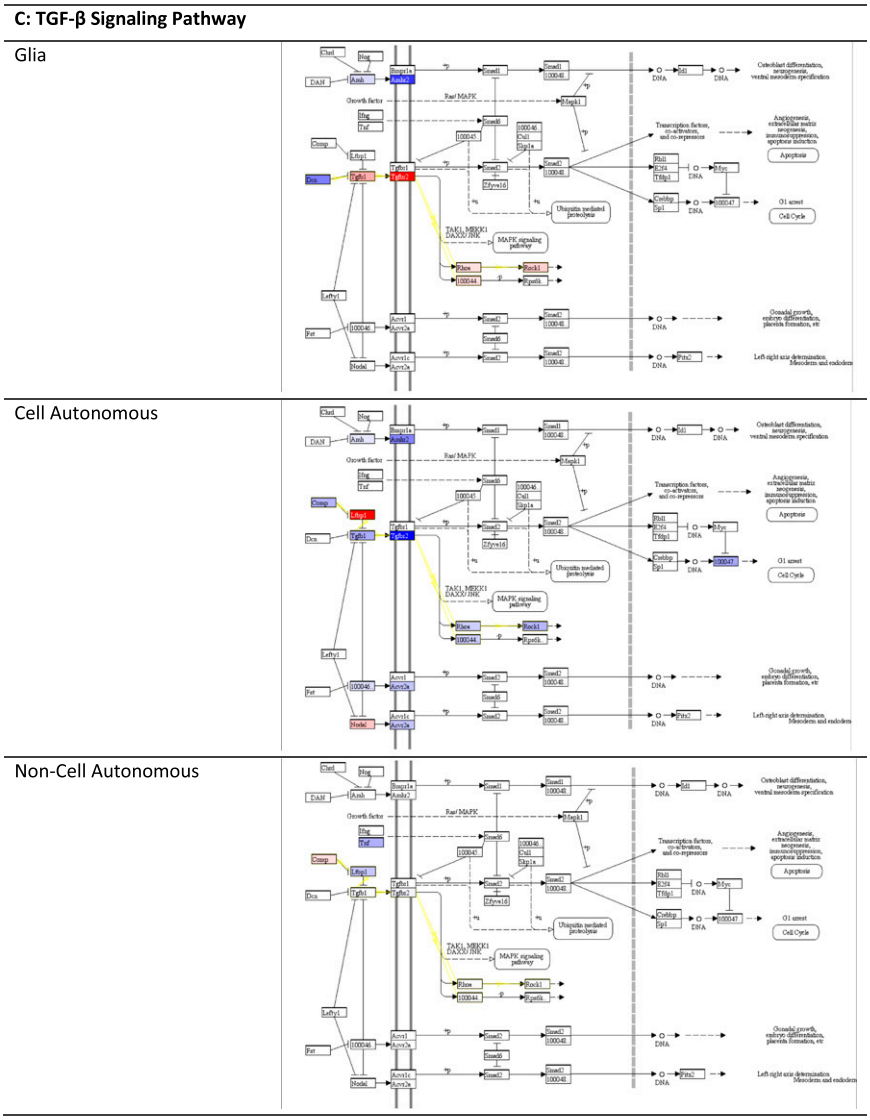

Fig. S4. KEGG pathways affected in neurons and glia. (*A*) ECM–receptor interaction. (*B*) Focal adhesion. (*C*) TGF-β pathway. Colors represent total accumulation as computed by Pathway Guide (*Materials and Methods*): red, up-regulated; blue, down-regulated; yellow lines, candidate mechanistic explanations for the observed perturbations.

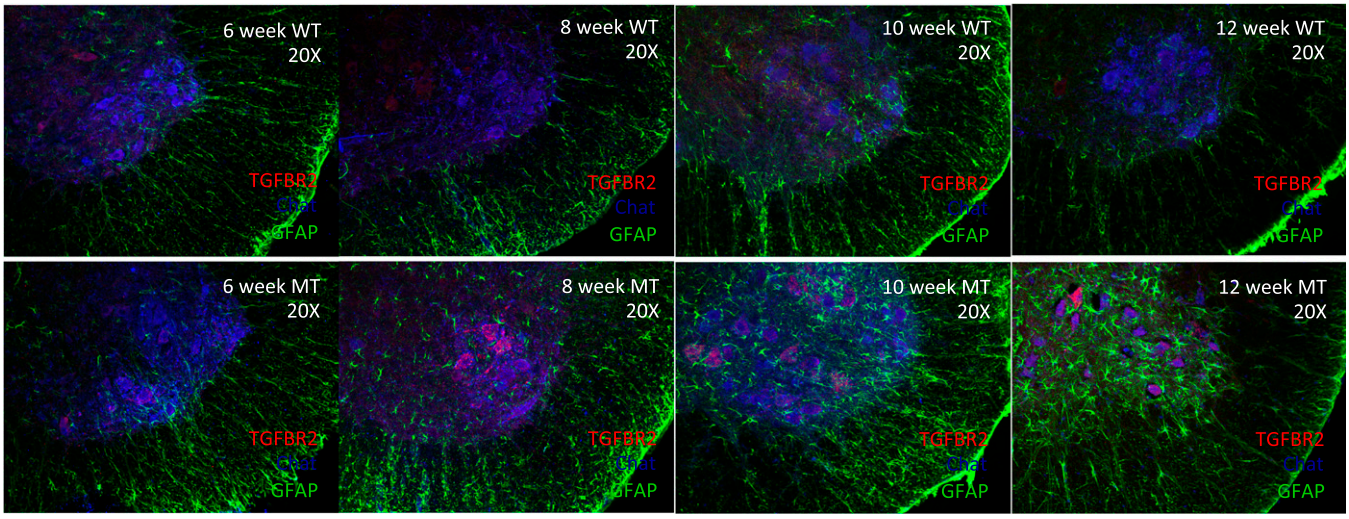

Fig. S5. Lumbar segments (L2–L5) of spinal cords from WT (*Upper*) and SOD1^{G93A} (*Lower*) mice immunostained against TGFβ-RII (red), which mainly colocalized with ventral horn-ChAT–positive neurons (blue, motor neurons). Images in *Lower* show the prevalence of TGFβ-RII–positive motor neurons during the disease progression. Abundance of reactive astrocytes (immunoreactivity against GFAP is shown in green) was used as an indicator of the disease condition.

Table S1. Primers sequences

		Direction	
Gene name	Product length	F	R
Clm1	165	ATTGCTGGTCCCCTTTCTCT	GGAACTCCTTGGCACCAGTA
Fzd10	159	TGGTACGCATAGGGGTCTTC	TCAGGCAGTCAGGTGTCTTG
Rundc1	205	GTCCTCACGTCCTGGGTTAC	TAGGCAAACGTCTCCAGGTC
Satb1	181	TTTAAAACACTCGGGCCATC	CAGCAACGCCATCTCTATCA
Serpinb5	152	CCCAGCAGGAAACATTCTCT	TGACTGTTTGAAACCCAAAGG
Spon1	187	GTGACGGACAGACCCATCTT	TGGCATACCCTCCATACTCC
Spon1	196	GTAACGAGGACCTGGAGCAG	CACTTCTTGCGTTGCACAGT
Uty	160	CAGCTTCTTCGGGTTCTTGA	TTCCAGTAAGAGATTGAAGTGACC
Wnt-11	187	CAGGATCCCAAGCCAATAAA	GACAGGTAGCGGGTCTTGAG
Wnt2b	175	ACTGGGGTGGCTGTAGTGAC	ACACCGTGACACTTGCACTC
Wnt-3	244	CAGCGTAGCAGAAGGTGTGA	TGGCCCCTTATGATGTGAGT

Other Supporting Information Files

Dataset S1 (XLSX)
Dataset S2 (XLSX)
Dataset S3 (XLSX)